Hierarchical Assembly of ZnO Nanostructures on SnO_2 Backbone Nanowires: Low-Temperature Hydrothermal Preparation and Optical Properties

Chuanwei Cheng,[†] Bo Liu,[†] Huiying Yang,[‡] Weiwei Zhou,[†] Li Sun,[†] Rui Chen,[†] Siu Fung Yu,[‡] Jixuan Zhang,[§] Hao Gong,[§] Handong Sun,[†] and Hong Jin Fan[†,*]

[†]Division of Physics and Applied Physics, School of Physical and Mathematical Sciences, Nanyang Technological University, 637371 Singapore, [‡]Division of Microelectronics, School of Electrical and Electronic Engineering, Nanyang Technological University, 639798 Singapore, and [§]Department of Materials Science and Engineering, National University of Singapore, 117576 Singapore

ABSTRACT Hierarchical nanostructures with SnO_2 backbones and ZnO branches are successfully prepared in a large scale by combining the vapor transport and deposition process (for SnO_2 nanowires) and a hydrothermal growth (for ZnO). The ZnO nanorods grow epitaxially on the SnO_2 nanowire side faces mainly with a four-fold symmetry. The number density and morphology of the secondary ZnO can be tailored by changing the precursor concentration, reaction time, and by adding surfactants. Photoluminescence (PL) properties are studied as a function of temperature and pumping power. Such hybrid SnO_2—ZnO nanostructures show an enhanced near-band gap emission compared with the primary SnO_2 nanowires. Under the optical excitation, a UV random lasing is observed which originates from the hierarchically assembled ZnO branches. These three-dimensional nanostructures may have application potentials as chemical sensors, battery electrodes, and optoelectronic devices.

KEYWORDS: nanowire · branch hierarchical · ZnO · SnO_2 · hydrothermal · lasing

One dimensional (1-D) nanomaterials, such as nanowires, nanorods, and nanotubes, are regarded as promising building blocks for future nanoscale devices and sensors. Driven by this, 1-D nanomaterials have been the focus of intensive research in recent years.[1−8] In particular, the hierarchical assembly of nanoscale building blocks with a tunable dimension and structure complexity is an essential step toward the realization of multifunctionality of nanomaterials when a large surface area is desired. Recently, there have been a number of reports on branched nanowires or complex 1-D nanowire arrays using a vapor transport and condensation method.[9−13] The synthesis strategies can be classified into two categories. The first one is a high-temperature thermal evaporation of precursor powders accompanied by a low-temperature condensation. Demonstrated materials include Zn_3P_2,[9] PbS,[10] ZnO,[11,12] and In_2O_3—ZnO.[13] In this one-step growth, 3-D hierarchical nanostructures form *via* a self-assembly (*e.g.*, self-catalytic secondary growth, screw dislocation driven growth). This method generally suffers from poor control and reproducibility because it is known that the morphology of the resulting nanomateirals in a vapor-transport-deposition process depends greatly on the vapor partial pressure, which can be hardly independently manipulated. The other hierarchization strategy consists of multiple vapor−liquid−solid (VLS) growths by reseeding the nanowire surface with catalyst (usually gold) nanoparticles. For examples, Dick *et al.* synthesized tree-like GaP nanostructures by metal−organic chemical vapor deposition (MOCVD).[14,15] Similarly, Wang and co-workers grew branched as well as hyperbranched Si nanowires.[16] Zai *et al.* fabricated rocketlike tetrapodal CdS nanorods and ZnS/SiO_2 core−shell structures by a seed-epitaxial route.[17,18] However, these methods require critical conditions: either high temperatures or special technique for catalyst attachment. Compared to the above methods, the solution-phase route is regarded as a less-costly and high-throughput way to the fabricate nanomaterials with the advantages of being environmentally friendly, low temperature, and simple. A variety of semiconductor composite nanomaterials with homo- or heterogeneous hierarchical structures have been

*Address correspondence to fanhj@ntu.edu.sg.

Received for review July 15, 2009 and accepted September 17, 2009.

Published online September 22, 2009.
10.1021/nn900848x CCC: $40.75

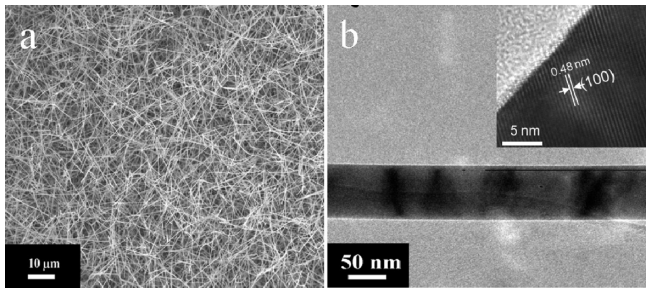

Figure 1. (a) SEM image of SnO_2 nanowires. (b) Typtical TEM image of a single SnO_2 nanowire. Inset is a HRTEM image of the wire showing its single-crystalline characteristics.

successfully prepared using this route in the past few years, such as CdTe,[19] ZnO,[20,21] Fe_2O_3/SnO_2,[22] and ZnO/TiO_2.[23]

Among the oxide semiconductors, ZnO and SnO_2 are well-known wide direct band gap (E_g = 3.37 and 3.6 eV at 300 K, respectively) semiconductors and possess wide application potentials in photovoltaics,[24,25] photocatalysis,[26] gas sensing,[27,28] and nanoscale laser source.[29] It has been demonstrated that, by combining ZnO and SnO_2, the heterojunction nanostructures, such core−shell tetrapods and wire-dots, can greatly enhance their application performance.[30−34] While the solution growth method allows a high degree of control, the resulting nanorods are usually short (~1 μm for >5 h). A vapor-phase growth has the advantage of a much faster growth rate, and the nanowires can be as long as 20 μm in a typical 1 h run. In this study, we combine these two growth processes to fabricate hierarchical SnO_2−ZnO nanostructures. First, a vapor-phase VLS route is employed to synthesize ultralong SnO_2 nanowires. Subsequently, ZnO nanorods are assembled epitaxially on the SnO_2 nanowires by a hydrothermal process. The main advantages of this method for obtaining complex ZnO nanostructures are the low growth temperature, so as to avoid thermally induced defects, and an absence of catalytic impurities, which is desirable when a high electric transport property is needed for sensor applications. The number density of the branches is easily changed by varying the precursor concentration. The strong near-band PL emission and a random lasing action support the excellent overall optical quality. Our demonstration of rational fabrication of hierarchical nanostructures may provide the possibility for designing more complex 3-D nanostructures with an ultrahigh surface area and subsequently exploiting their unique physical properties.

RESULTS AND DISCUSSION

ZnO Nanorod Arrays on SnO_2 Nanowire Backbones. Figure 1 shows the SEM and TEM images of the primary SnO_2 nanowires. The nanowires have a diameter of 50−100 nm and length of several tens of micrometers, with a relative smooth surface.

After applying the solution growth of ZnO nanorods, the initially smooth SnO_2 nanowires branch out, forming a hierarchical structure resembling the leaves of a pine tree. A typical image of such structure is shown in Figure 2a. The nanorod branches stand perpendicular to the side surfaces of the SnO_2 nanowires as multiple rows in a parallel manner. In general, the SnO_2 nanowire backbones can be as long as tens of micrometers, whereas the length of the secondary ZnO nanorods grown on the SnO_2 backbone ranges from 100 to 200 nm and the diameter of about 30 nm. While the majority of the hybrid nanostructures have four-fold symmetry branches, a few six-fold symmetry nanowires were also observed.

The structure was further examined using transmission electron microscopy (TEM). The TEM image in Figure 2b shows a portion of the SnO_2/ZnO hierarchical nanostructure. The ZnO nanorods are not of uniform diameter, which is characteristic of solution-grown ZnO nanorods. It is noted that some branches were broken off from the trunk by sonication during the TEM sample preparation process. Figure 2c,d presents the energy-dispersive X-ray spectroscopy (EDS) spectra taken from the backbone and one branch in Figure 2b, respectively. Clearly, all of the secondary nanorods are pure ZnO, and the major core is SnO_2; the C and Cu element signals are attributed to the TEM grid used to support the nanowire.

Now we come closer to the interface between the SnO_2 backbone and ZnO branch. Figure 3a displays the interface region of one branch, from which the HRTEM image was recorded (white frame area in Figure 3a). Both the branch and the backbone are single-crystalline with clear lattice fringes. The lattice spacings of 0.269 nm for the branch nanorods and 0.48 nm for the backbone nanowires correspond, respectively, to the (0002) plane of the wurtzite ZnO and the (100) plane of rutile SnO_2 (more details can be found in Supporting Information, Figure S1). Supporting Information is given by selective area electron diffraction pattern of the branch (Figure 3c) and two-dimensional fast Fourier transforms (FFT) of the lattice image of the backbone (Figure 3d). ZnO nanorods grew perpendicular to the longitudinal axis of the SnO_2 nanowire with an interfacial orientation relationship of (0002)ZnO‖(−101)SnO_2. It is well-known that lattice mismatch plays an important role in the expitaxial growth of heterogeneous structures either in vapor-phase deposition[9] or solution-phase epitaxial growth.[13] A high degree of lattice mismatch prevents the nucleation and growth of an overlayer on a substrate because of the high structural strain. In our case, the main interface relation for hierarchical nanostructures is (0002)ZnO‖(−101)SnO_2 (as revealed by HRTEM and SAED). The structure model for atomic arrangement

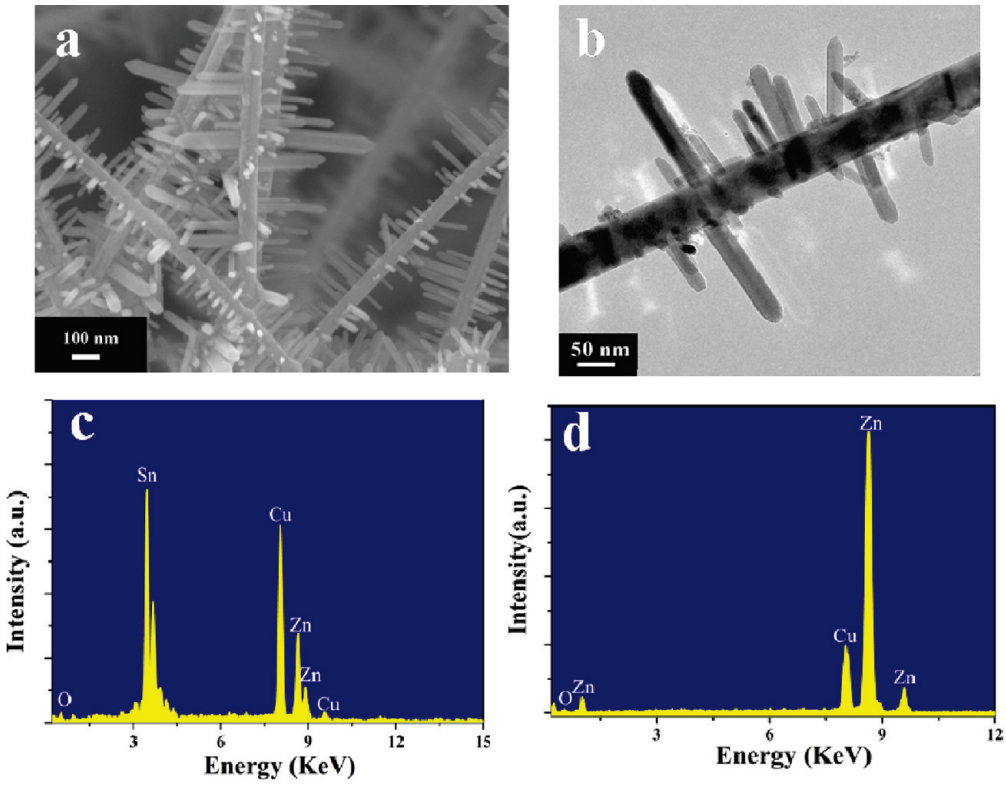

Figure 2. Hierarchical SnO_2/ZnO nanostructures with ZnO nanorod branches on SnO_2 nanowire backbones. (a) SEM image. (b) Typical TEM image. (c,d) Energy-dispersive spectrum (EDS) recorded from the SnO_2 trunk and one ZnO nanorod branch in Figure 2b, respectively. Note that the oxygen peak is not present, which is artificial.

(see Supporting Information, Figure S2) shows lattice mismatches of 1.9 and 5.6% along the *b* direction and *a* direction of SnO_2, respectively. Therefore, the ZnO nanocrystals, which tend to elongate along the [0002] direction during the solution growth, prefer to nucleate and grow on the four {101} planes of SnO_2 nanowire backbones. This contributes to the formation of four-fold symmetry branches.

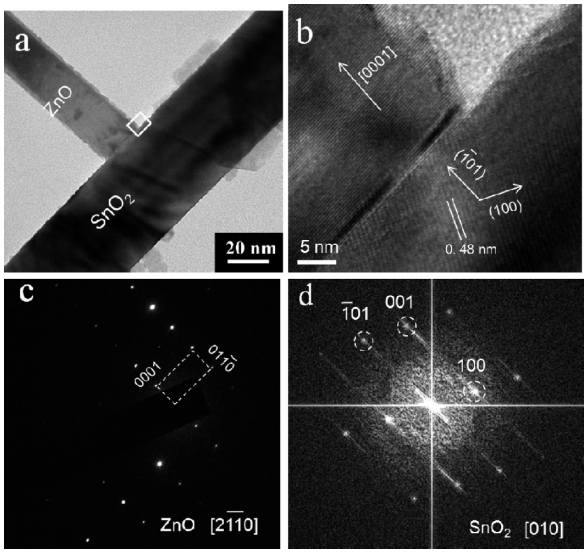

Figure 3. Structural characterization of the heterointerface. (a) TEM image taken near the junction. (b) HR lattice image of the junction. (c) Electron diffraction pattern taken from the ZnO nanorod branches. (d) Fast Fourier transformation pattern of the HRTEM of the SnO_2 backbone in (b). The electron beam directions (right-bottom in c and d) are calculated based on indexed planes.

X-ray diffraction (XRD) analysis was performed to investigate the crystal phase of SnO_2 nanowires and SnO_2/ZnO hierarchical structures in Figure 2. Figure 4 illustrates the XRD patterns of both the primary SnO_2 nanowires (curve 1) and the hybrids (curve 2) for comparison. Clearly, the crystal phase of SnO_2 used as the backbone is rutile phase (space group: $P42/mnm$, $a = 0.4739$ nm, $c = 0.3186$ nm). As for the SnO_2/ZnO hybrids, all of the diffraction peaks can be indexed as a mixture of hexagonal wurtzite ZnO (space group: $P63/mc$, $a = 0.3249$ nm, $c = 0.5206$ nm) and the tetragonal rutile SnO_2, which is consistent to the JCPDS file Nos. 079-2205 and 071-0652, respectively. No remarkable shift in diffraction peak was detected. This indicates that no obvious interface reaction of $ZnO + SnO_2 \rightarrow Zn_2SnO_4$ has occurred.

Nano-ZnO is known to exhibit a large variety of morphologies and interesting size and morphology-dependent physical properties.[3,20] Therefore, a growth control of the nanostructure has always been a critical issue. In our experiment, the morphology of the secondary ZnO nanostructures is tailored by changing the liquid

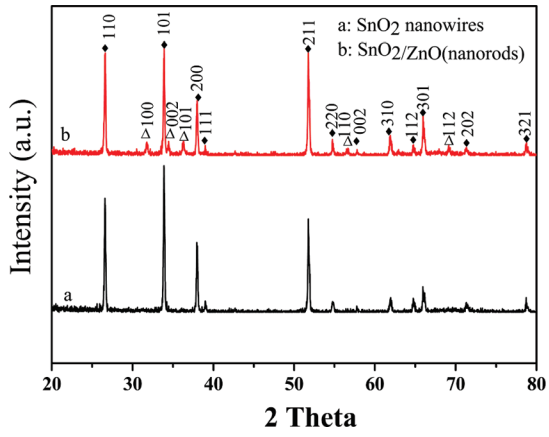

Figure 4. XRD patterns of the primary SnO_2 nanowires (curve a) and SnO_2/ZnO hybrids with ZnO nanorods grown on SnO_2 nanowires (curve b); ♦ indicates the rutile phase of SnO_2, and Δ indicates the wurtzite phase of ZnO.

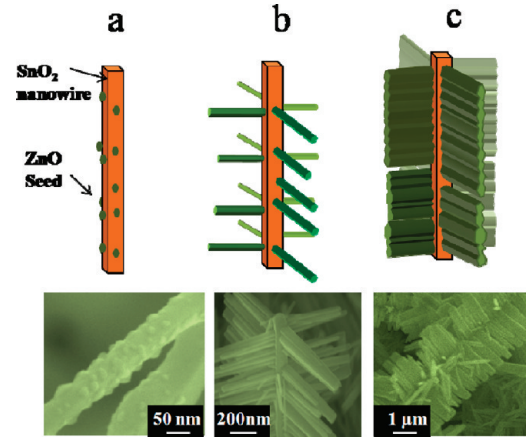

Figure 6. Growth process of the SnO_2/ZnO hierarchical nanostructures. Top row: schematics. Bottom row: corresponding SEM images of the product. (a) Before the growth. The SnO_2 nanowire surfaces are coated with ZnO seed nanoparticles. Subsequent solution epitaxial growth of ZnO nanorods on the four side faces of SnO_2 nanowires. (b) With a low $Zn(NO_3)_2$ precursor concentration, the branches are individual ZnO nanorod arrays, whereas (c) with a high precursor concentration, the nanorods tend to merge.

precursor concentrations or adding additives during the hydrothermal process. Figure 5a−d shows the representative SEM images of hierarchical SnO_2/ZnO nanostructures by increasing the concentration of $Zn(NO_3)_2$ salts and hexmethylenetetramine (HMT), while keeping their ratio of 1:1 unchanged. Obviously, both the density and diameter of the secondary ZnO nanorods increase directly monotonously with the concentration of salts. For example, the diameter of the nanorods varied in the range of 30−200 nm and the length of 200−1000 nm by increasing the zinc nitrate salt concentration from 0.01 to 0.1 M.

Figure 6 shows schematically the two-step growth process employed in our experiment together with SEM images of the structures obtained under the respective growth condition. First, the pristine SnO_2 nanowires were attached by dip coat-

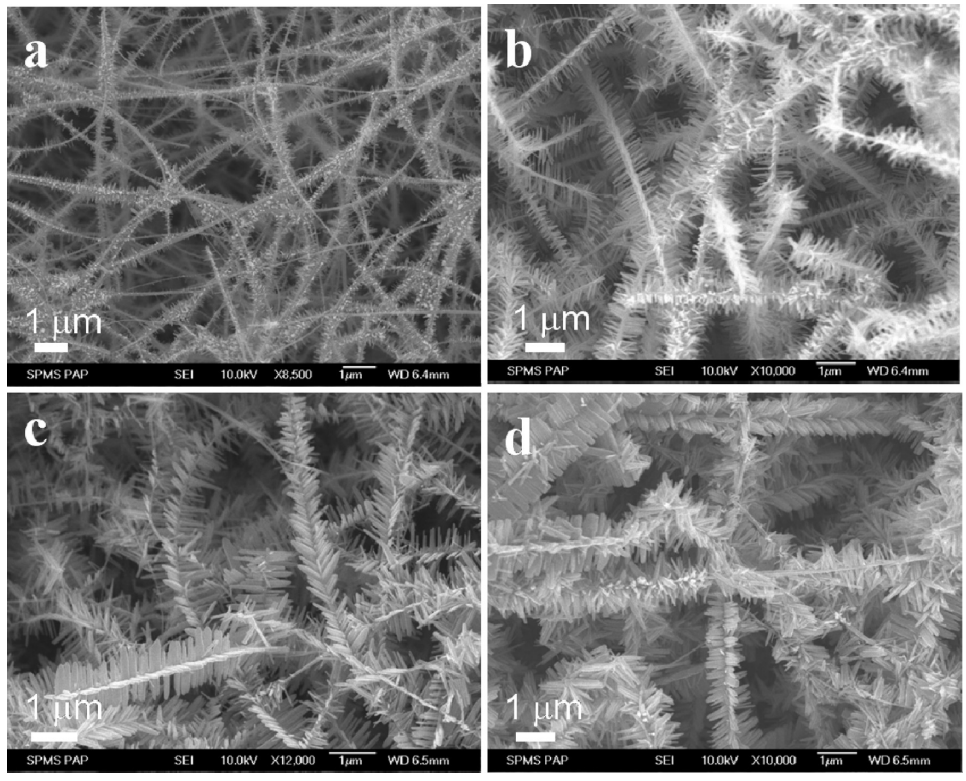

Figure 5. Growth manipulation of the SnO_2/ZnO hierarchical nanostructures by using different concentrations of $Zn(NO_3)_2$ salts for 8 h: (a) 0.01 M, (b) 0.025 M, (c) 0.05 M, (d) 0.1 M.

ing with a layer of ZnO seed nanoparticles as specific nucleate sites. Such a layer of ZnO nanoparticles of a diameter of ~5 nm on the surface of SnO_2 nanowires can be seen from the SEM image (Figure 6a). It is noted that the seed layer is mandatory because no secondary growth was observed when this step was omitted (see Supporting Information, Figure S3). In the early stage, ZnO nanorods nucleate and crystallize along their [0001] direction on the ZnO seed sites. With time increases, the initial nanorods absorb Zn^{2+} and OH^- from the solution and crystallize following the well-documented chemical reactions in the presence of zinc salts and HMT[35]

$$(CH_2)_6N_4 + 6H_2O \xrightarrow{\Delta} 6HCHO + 4NH_3 \quad (1)$$

$$NH_3 + H_2O \rightleftarrows NH_4^+ + OH^- \quad (2)$$

$$2OH^- + Zn^{2+} \rightarrow Zn(OH)_2 \rightarrow ZnO_{(s)} + H_2O \quad (3)$$

A series of time-dependent experiments were conducted for a clear illustration of the growth process (see Supporting Information, Figure S4). After a short growth of 0.5 h, ZnO crystals sprouting from the seeds are evident. Extending the reaction to 6 h resulted in four rows of ZnO nanorods with a length of ~200 nm (Figure 6b). Under the condition of a higher zinc salt concentration, the lateral growth of ZnO nanorods competes, which reduces the anisotropy of the resulting structure. This is consistent with the pioneering work by Vayssieres.[35] Subsequently, the nanorods grow thicker and tend to merge *via* a gap-filling growth,[36] as shown in Figure 6c.

ZnO Nanosheets on SnO_2 Nanowire Backbone. Further modification of the branch structures was made by adding trisodium citrate as the surfactant into the hydrothermal solution. The results of the products are shown in Figure 7. Instead of 1-D structure under the surfactant-free condition, layers of ZnO nanoflakes on the SnO_2 nanowires were obtained. Electron microscopy examination (Figure 7a−c) reveals that the ZnO nanoflakes are <5 nm in thickness and overall size of ~200 nm. They are also of wurtzite phase, as shown by XRD result (Supporting Information, Figure S5). It is reasonable to expect that the wide planes of the sheets are (0001) planes.

ZnO crystal is a polar crystal consisting of many positive polar planes (rich in Zn^{2+}) and negative polar planes (rich in O^{2-}).[37] In general, in the absence of structure modifiers under hydrothermal condition, the (0001) polar plane is energetically unfavorable and has a faster growth rate than other planes. Therefore, ZnO tends to grow into rodlike crystals in an aqueous system. However, when certain structure modifying agent is added, such as trisodium citrate in this case, the citrate molecule may be adsorbed preferentially on the energetically unfavorable (0001) polar suface.[38] The absorbed molecules will reduce the surface energy of the (0001) plane and thus retard the growth along the [0001] orientation. As a result, hexagonal-shaped ZnO nanoflakes with (0001) flat planes were formed.

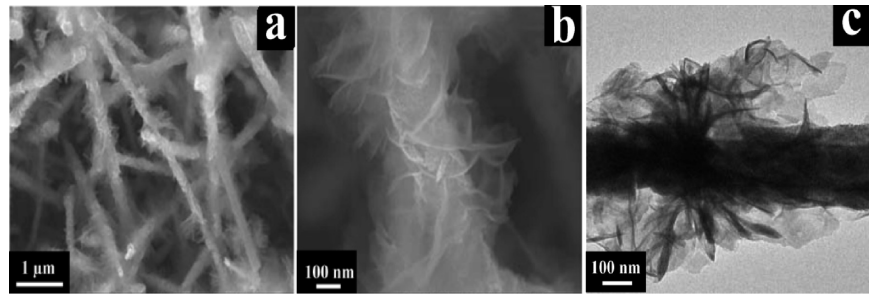

Figure 7. SnO_2/ZnO hierarchical structures with ZnO nanoflakes grown on SnO_2 nanowires by adding trisodium citrate. (a) Low- and (b) high-magnification SEM images. (c) TEM image.

Photoluminescence Properties. The optical characteristics of the SnO_2 nanowires and SnO_2/ZnO hierarchical structures were investigated by photoluminescence (PL) spectroscopy at various temperatures between 10

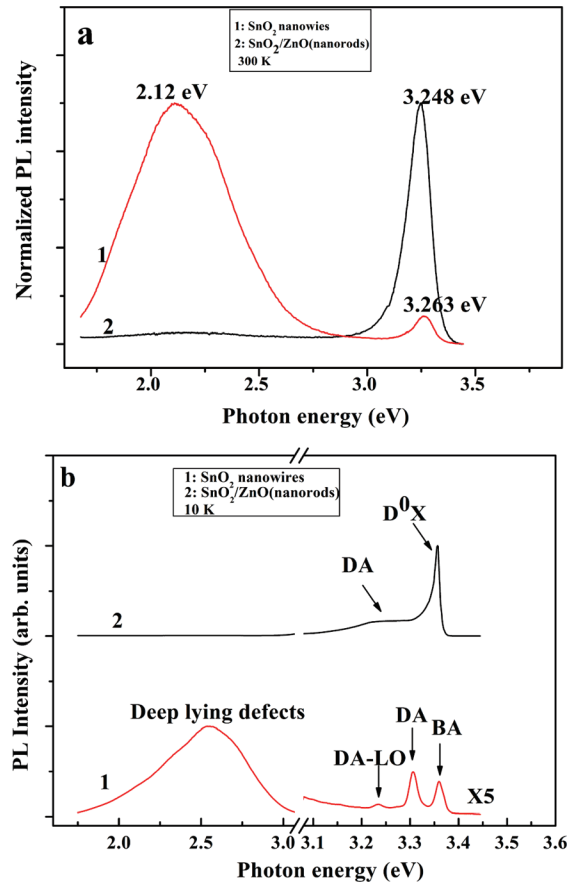

Figure 8. Photoluminescence (PL) spectra of the primary SnO_2 nanowires (curve 1) and SnO_2/ZnO hybrids with ZnO nanorod branches (curve 2) recorded at (a) room temperature and (b) 10 K.

K and room temperature. As shown in Figure 8a, the room-temperature PL spectrum of the primary SnO_2 nanowires (curve 1) consists of a broad emission band centered at ~2.12 eV, which is ascribed to deep level defects, and a weak UV emission at 3.263 eV. As for the SnO_2/ZnO hierarchical structures, the PL spectrum is dramatically different compared with the primary SnO_2 nanowires. The intensity of defect-related emission from SnO_2 is remarkably suppressed after attaching with the ZnO nanorods. In addition, a dominating near-band-edge (NBE) emission at 3.248 eV from ZnO was observed.

To further confirm the origin of the PL peaks, low-temperature measurement was conducted. The 10 K PL spectra of both primary SnO_2 nanowires and the hybrids are shown in Figure 8b. For the pure SnO_2 nanowire samples, four peaks at 3.359, 3.306, 3.233 eV, and the broad emission at 2.54 eV can be clearly seen in curve 1. The 3.359 and 3.306 eV peaks are assigned to the band to acceptor (BA) and donor to acceptor (DA) emission, respectively, which are consistent with previous reports for bulk tin oxide[39] and tin oxide nanowires.[40] As the 3.233 eV peak differs from the DA emission by 73 meV, the former is believed to be a LA-phonon replica of DA.[40] The broad emission at 2.54 eV is due to deep lying defects. On this basis, we can conclude that the room-temperature weak UV emission peak at 3.263 eV from the primary SnO_2 nanowires (curve 1 in Figure 8a) originates from the suppression of several NBE bands such as BA and DA peaks (see curve 1 in Figure 8b); it is shifted due to the band gap narrowing with increasing temperature. While for the SnO_2/ZnO hierarchical structures (curve 2 in Figure 8b), the dominant peak at 3.358 eV is attributed to the neutral donor-bound excitons in the ZnO nanorods,[41] the peaks at lower energy are assigned to donor−acceptor pair recombination.[41,42] Also, a very weak green emission peak due to oxygen deficiency was also observed.

Temperature-dependent PL spectra of the SnO_2/ZnO hierarchical structures were also measured in the range of 10−300 K. As shown in Figure 9, the PL peaks at 3.357 eV, attributed to donor-bound excitons of ZnO, dominate the spectra at low temperature. By increasing the temperature, the bound excitons disassociate into free excitons and the corresponding peak red shifts as a function of increasing temperature. Such property is well-established in ZnO published in both films and nanostructures.

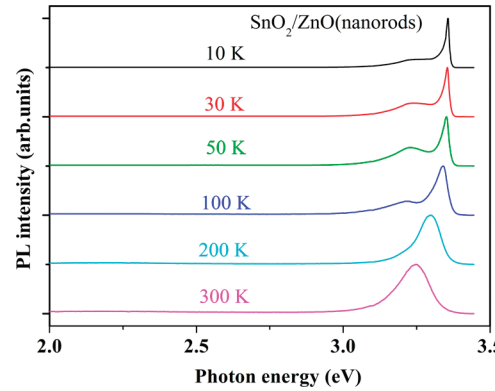

Figure 9. Temperature-dependent PL spectra of the SnO_2/ZnO hybrid nanostructures.

It is interesting to notice that the PL peaks of the SnO_2 backbone are missing for the hybrid nanostructures. We propose two reasons for this: first, the secondary-grown ZnO nanorods compensated the defects on the surface of the SnO_2 nanowires (*e.g.*, oxygen vacancies), so that the surface state related emissions at ~2 eV were decreased. Second, as the UV light penetration depth in ZnO was less than 100 nm,[43] which is smaller than the length of ZnO nanorods assembled on the SnO_2 nanowire surface, the majority of the UV laser power would be absorbed by the ZnO nanorod branches (note the band gap of ZnO).

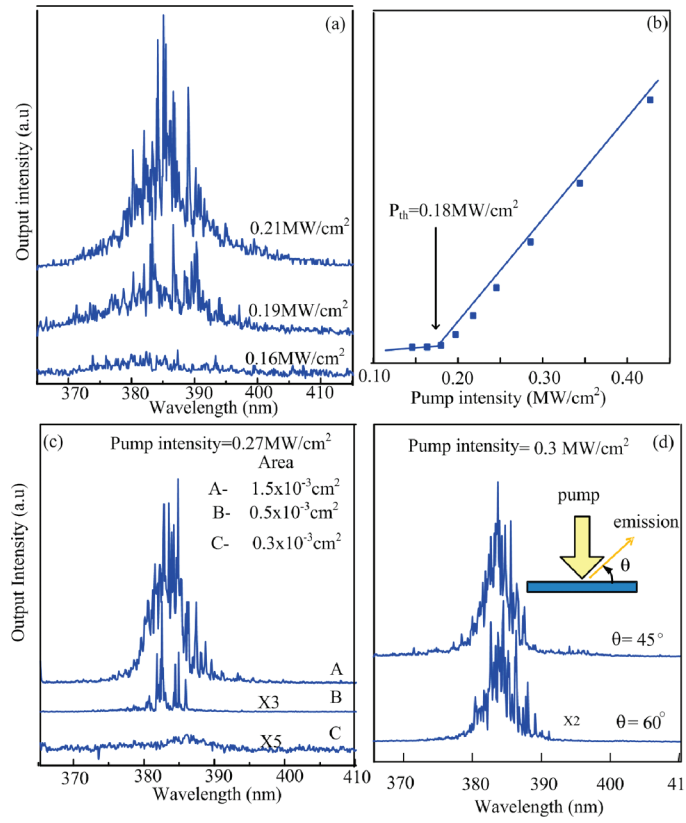

Figure 10. Random lasing action of the SnO_2/ZnO hierarchical nanostructures. (a) Room-temperature PL spectra at different excitation powers. (b) Plot of integrated intensity *versus* input power intensity, showing the onset of nonlinearity at a threshold of ~0.18 MW/cm^2. (c) Emission spectra of the sample with different excitation area. (d) Spectra radiated from 45 and 60° from the sample surface.

Therefore, the intensity of NBE of the SnO_2 backbone, which is already weak (see curve 1 in Figure 8a), was significantly suppressed.

Random Lasing Emission. It is expected that such 3-D hierarchical assembly should enhance the random lasing action of ZnO nanostructures, compared to those unidirectional ordered arrays.[29,44] Figure 10a,b shows the emission spectra and light−light curve, respectively, of the SnO_2/ZnO hybrid nanowires. It is observed that, when excitation power exceeds a threshold of ~0.18 MW/cm^2, sharp peaks in a line width as narrow as 0.4 nm emerged from the single, broad spontaneous emission spectrum. The intensities of the sharp peaks are significantly higher than the background noise level, whereas their positions are found to be independent with the pumping intensity. As the pump power increased, multiple laser modes with strong coherent feedback at wavelengths between 380 and 390 nm were detected. Figure 10c shows the variation of emission spectra with excitation area for constant pump intensity of 0.27 MW/cm^2. It is observed that, when the excitation area is less than critical area (~0.3×10^{-3} cm^2), no more sharp lasing peak can be observed. Furthermore, emission spectra measured at different observation angles are plotted in Figure 10d. It is noted that different emission spectra can be observed in different directions. These properties of emission spectra are qualitatively consistent with the random lasing behavior with a coherent feedback.[45,46]

CONCLUSIONS

We have reported a series of ZnO nanostructures hierarchically assembled on SnO_2 nanowire backbones through a low-temperature heteroepitaxy growth in an aqueous solution. The number density and morphology of secondary ZnO nanostructure can be tuned by adjusting the baking condition, such as the salt concentration, reaction time, and additives. Interestingly, the as-synthesized SnO_2/ZnO hybrid nanostructures exhibit unique luminescence properties in contrast to the primary SnO_2 nanowires: the defect emission from SnO_2 at ~580 nm is significantly suppressed, whereas a strong UV emission coming from ZnO is observed. Moreover, this type of 3-D structure emits lasing peaks that are stronger than those from the pristine nanowires. Such lasing emission is identified as multimode random lasing, which is correlated with the hierarchical assembly and spatial 3-D arrangement of the ZnO nanorods. We claim that the present two-step approach for epitaxial growth of hierarchical nanostructures can be extended to designing other complex systems (using nanowires or tubes as a template), which might be useful for applications in laser, gas sensors, and solar energy conversion devices.

EXPERIMENTAL SECTION

Synthesis of SnO_2 Nanowires. SnO_2 nanowires were synthesized on silicon substrates by a vapor transport and deposition process. An equal amount of SnO_2 powder (Sigma Aldrich, 99.9%) and graphite powder (Sigma Aldrich, 99%) was grounded and transferred to an alumina boat. The Au sputter-coated Si substrates and the alumina boat were placed in a small quartz tube (diameter 15 mm, length 300 mm). The substrates were typically placed 1−4 cm away from the center of the boat. This quartz tube was then placed inside a furnace quartz tube, with the center of the alumina boat positioned at the center of the furnace and the substrates placed downstream of an argon flow. The temperature of the furnace was ramped to 1050 °C at a rate of 50 °C /min and kept at that temperature for 1 h under a constant flow of argon (50 sccm) and pressure (15 mbar). After the furnace cooled to room temperature, the substrate surface turned to white or a light gray color, indicating the deposition of materials.

SnO_2/ZnO Hierarchical Structure Fabrication. SnO_2/ZnO hierarchical structures were prepared by a hydrothermal process. First, the SnO_2 nanowires were coated with ZnO nanoparticles as seeds by a dip-coating technique.[47] Subsequently, the SnO_2 nanowire-covered substrates were immersed into a 35 mL aqueous solution of equimolar zinc nitrate ($Zn(NO_3)_2 \cdot 6H_2O$) and hexamethylenetetramine ($C_6H_{12}N_4$). The hydrothermal process was conducted at 95 °C for 8 h. After reactions, the substrates were removed from the solution, rinsed with deionized water, and dried with Ar blow.

Characterizations. The morphology and the crystalline structure of the as-fabricated SnO_2/ZnO heterostructures were characterized with a JEOL JSM-6700F field emission scanning electron microscope (FESEM) and a JEM 2010F high-resolution transmission electron microscope (HR-TEM). X-ray powder diffraction (XRD) patterns were recorded on a Bruker D8 Advance diffractometer using Cu Kα radiation. The PL measurement was performed from 10 K to room temperature using the 325 nm line of a continuous-wave He−Cd laser as the excitation source. Lasing emission of the samples was investigated under an optical excitation by a 355 nm frequency-tripled (Nd:YAG yttrium aluminum garnet) pulse laser with 120 ps pulse width and 10 Hz repetition rate. The optical pumping was achieved by using a cylindrical lens to focus a pump stripe of 2 mm in length and 40 μm in width onto the sample.

Acknowledgment. This work is supported by the start-up funding from Nanyang Technological University to H.J.F.

Supporting Information Available: SEM image of the nanowires after the ZnO hydrothermal growth with a seed layer, an enlarged HRTEM of the interface (Figure 3b), time-dependent growth experiments showing the structural evolution of the branches, and XRD spectrum of the hybrid structure with ZnO nanosheets. This material is available free of charge *via* the Internet at http://pubs.acs.org.

REFERENCES AND NOTES

1. Hu, J. T.; Odom, T. W.; Lieber, C. M. Chemistry and Physics in One Dimension: Synthesis and Properties of Nanowires and Nanotube. *Acc. Chem. Res.* **1999**, *32*, 435–445.
2. Fan, H. J.; Werner, P.; Zacharias, M. Semiconductor Nanowires: From Self-Organization to Patterned Growth. *Small* **2006**, *2*, 700–717.
3. Wang, Z. L. ZnO Nanowires and Nanobelts Platforms for Nanotechnology. *Mater. Sci. Eng. Rep.* **2009**, *64*, 33–71.
4. Duan, X. F.; Huang, Y.; Cui, Y.; Wang, J.; Lieber, C. M. Indium Phosphide Nanowires as Building Blocks For Nanoscale Electronic and Optoelectronic Devices. *Nature* **2001**, *409*, 66–69.
5. Li, Y.; Qian, F.; Xiang, J.; Lieber, C. M. Nanowire Electronic and Optoelectronic Devices. *Mater. Today* **2006**, *9*, 18–25.
6. Bao, J. M.; Zimmler, M. A.; Capasso, F. Broadband ZnO Single-Nanowire Light-Emitting Diode. *Nano Lett.* **2006**, *6*, 1719–1722.

7. Duan, X. F.; Huang, Y.; Argarawal, R.; Lieber, C. M. Single-Nanowire Electrically Driven Lasers. *Nature* **2002**, *421*, 241–245.
8. Kong, J.; Franklin, N. R.; Zhou, C. W.; Chapline, M. G.; Peng, S.; Cho, K.; Dai, H. J. Nanotube Molecular Wires as Chemical Sensors. *Science* **2000**, *287*, 622–625.
9. Yang, R.; Chueh, Y. L.; Morber, J. R.; Snyder, R.; Chou, L. J.; Wang, Z. L. Single-Crystalline Branched Zinc Phosphide Nanostructures: Synthesis, Properties, and Optoelectronic Devices. *Nano Lett.* **2007**, *7*, 269–275.
10. Matthew, J. B.; Y. K. Albert, L.; Alexander, V. K.; Andrew, L. S.; Song, J. Dislocation-Driven Nanowire Growth and Eshelby Twist. *Science* **2008**, *320*, 1060–1063.
11. Gao, P. X.; Wang, Z. L. Self-Assembled Nanowire-Nanoribbon Junction Arrays of ZnO. *J. Phys. Chem. B* **2002**, *106*, 12563–12658.
12. Yan, H.; He, R.; Johnson, J.; Law, M.; Saykally, R. J.; Yang, P. D. Dendritic Nanowire Ultraviolet Laser Array. *J. Am. Chem. Soc.* **2003**, *125*, 4728–4729.
13. Lao, J.; Wen, J.; Ren, Z. F. Hierarchical ZnO Nanostructures. *Nano Lett.* **2002**, *2*, 1287–1291.
14. Dick, K. A.; Deppert, K.; Martensson, T.; Seifert, W.; Samuelson, L. Growth of GaP Nanotree Structures by Sequential Seeding of 1D Nanowires. *J. Cryst. Growth* **2004**, *272*, 131–137.
15. Dick, K. A.; Deppert, K.; Larsson, M. W.; Martensson, T.; Seifert, W.; Wallenberg, L. R.; Samuelson, L. Synthesis of Branched 'Nanotrees' by Controlled Seeding of Multiple Branching Events. *Nat. Mater.* **2004**, *3*, 380–384.
16. Wang, D. L.; Qian, F.; Yang, C.; Zhong, Z. H.; Lieber, C. M. Rational Growth of Branched and Hyperbranched Nanowire Structures. *Nano Lett.* **2004**, *4*, 871–874.
17. Zhai, T. Y.; Gu, Z. J.; Zhong, H. Z.; Dong, Y.; Ma, Y.; Fu, H. B.; Li, Y. F.; Yao, J. N. Design and Fabrication of Rocketlike Tetrapodal CdS Nanorods by Seed-Epitaxial Metal-Organic Chemical Vapor Deposition. *Cryst. Growth Des.* **2007**, *7*, 488–491.
18. Zhai, T. Y.; Gu, Z. J.; Dong, Y.; Zhong, H. Z.; Ma, Y.; Fu, H. B.; Li, Y. F.; Yao, J. N. Synthesis and Cathodoluminescence of Morphology-Tunable SiO_2 Nanotubes and ZnS/SiO_2 Core−Shell Structures Using CdSe Nanocrystals as the Seeds. *J. Phys. Chem. C.* **2007**, *111*, 11604–11611.
19. Manna, L.; Milliron, D. J.; Meisel, A.; Scher, E. C.; Alivisatos, A. P. Controlled Growth of Tetrapod-Branched Inorganic Nanocrystals. *Nat. Mater.* **2003**, *2*, 382–385.
20. Zhang, T. T.; Dong, W. J.; Brewer, M. K.; Konar, S.; Njabon, R. N.; Tian, Z. R. Site-Specific Nucleation and Growth Kinetics in Hierarchical Nanosyntheses of Branched ZnO Crystallites. *J. Am. Chem. Soc.* **2006**, *128*, 10960–10968.
21. Sounart, T. L.; Liu, J.; Voigt, J. A.; Huo, M.; Spoerke, E. D.; Mckenzie, B. Secondary Nucleation and Growth of ZnO. *J. Am. Chem. Soc.* **2007**, *129*, 15786–15793.
22. Zhang, D. F.; Sun, L. D.; Jia, C. J.; Yan, Z. G.; You, L. P.; Yan, C. H. Hierarchical Assembly of SnO_2 Nanorod Arrays on Fe_2O_3 Nanotubes: A Case of Interfacial Lattice Compatibility. *J. Am. Chem. Soc.* **2005**, *127*, 13492–13493.
23. Wang, N. X.; Sun, C. H.; Zhao, Y.; Zhou, S. Y.; Chen, P.; Jiang, L. Fabrication of Three-Dimensional ZnO/TiO_2 Heteroarchitectures *via* a Solution Process. *J. Mater. Chem.* **2008**, *18*, 3909–3911.
24. Lorie, M.; Johnson, G. J.; Saykally, R.; Yang, P. D. Nanowire Dye-Sensitized Solar Cells. *Nat. Mater.* **2005**, *4*, 455–459.
25. Gubbala, S.; Chakrapani, V.; Kumar, V.; Sunkara, M. K. Band-Edge Engineered Hybrid Structures for Dye-Sensitized Solar Cells Based on SnO_2 Nanowires. *Adv. Funct. Mater.* **2008**, *18*, 2411–2418.
26. Wang, W. W.; Zhu, Y. J.; Yang, L. X. ZnO−SnO_2 Hollow Spheres and Hierarchical Nanosheets: Hydrothermal Preparation, Formation Mechanism, and Photocatalytic Properties. *Adv. Funct. Mater.* **2007**, *17*, 59–64.
27. Cheng, C. W.; Xu, G. Y.; Zhang, H. Q.; Luo, Y. Fabricating ZnO Nanorods Sensor for Chemical Gas Detection at Room Temperature. *J. Nanosci. Nanotechnol.* **2007**, *7*, 4439–4442.
28. Wang, Y. L.; Jiang, C. C.; Xia, Y. N. Precursor Route to Polycrystalline SnO_2 Nanowires That Can Be Used for Gas Sensing under Ambient Conditions. *J. Am. Chem. Soc.* **2003**, *125*, 16176–16177.
29. Huang, M. H.; Mao, S.; Feick, H.; Yan, H. Q.; Wu, Y. Y.; Kind, H.; Weber, E.; Russo, R.; Yang, P. D. Room-Temperature Ultraviolet Nanowire Nanolaser. *Science* **2001**, *292*, 1897–1899.
30. Kuang, Q.; Jiang, Z. Y.; Xie, Z. X.; Lin, S. C.; Lin, Z. W.; Xie, S. Y.; Huang, R. B.; Zheng, L. S. Tailoring the Optical Properties by a Three Dimensional Epitaxial Heterostructure. *J. Am. Chem. Soc.* **2005**, *127*, 11777–11784.
31. Zhao, J. W.; Ye, C. H.; Fang, X. S.; Qin, L. R.; Zhang, L. D. Selective Growth of Crystalline SnO_2 on the Polar Surface of ZnO Nanobelts. *Cryst. Growth Des.* **2006**, *6*, 2643–2647.
32. Kuang, Q.; Lao, C. S.; Li, Z.; Liu, Z. Y.; Xie, Z. X.; Zheng, L. S.; Wang, Z. L. Enhancing the Photon- and Gas-Sensing Properties of a Single SnO_2 Nanowire Based Nanodevice by Nanoparticle Surface Functionalization. *J. Phys. Chem. C* **2008**, *112*, 11539–11544.
33. Zheng, L. R.; Zheng, Y. H.; Chen, C. Q.; Zhan, Y. Y.; Lin, X. Y.; Zheng, Q.; Wei, K. M.; Zhu, J. F. Network Structured SnO_2/ZnO Heterojunction Nanocatalyst with High Photocatalytic Activity. *Inorg. Chem.* **2009**, *48*, 1819–1825.
34. Wang, J. X.; Sun, X. W.; Xie, S. S.; Yang, Y.; Chen, H. Y.; Lo, G. Q.; Kwong, D. L. Preferential Growth of SnO_2 Triangular Nanoparticles on ZnO Nanobelts. *J. Phys. Chem. C* **2007**, *111*, 7671–7675.
35. Vayssieres, L. Growth of Arrayed Nanorods and Nanowires of ZnO from Aqueous Solution. *Adv. Mater.* **2003**, *15*, 464–466.
36. Fan, H. J.; Zacharias, M. Manipulation of Crawling Growth for the Formation of Sub-Millimeter Long ZnO Nanowalls. *J. Mater. Sci. Technol.* **2008**, *24*, 589–593.
37. Wang, Z. L.; Kong, X. Y.; Zuo, J. M. Induced Growth of Asymmetric Nanocantilever Arrays on Polar Surfaces. *Phys. Rev. Lett.* **2003**, *91*, 185502–185505.
38. Tian, Z. R.; Voigt, J. A.; Liu, J.; Mckenzie, B.; Mcdermott, M. J.; Rodriguez, M. A.; Konishi, H.; Xu, H. F. Complex and Oriented ZnO Nanostructures. *Nat. Mater.* **2003**, *2*, 821–826.
39. Blattner, G.; Klingshrin, C.; Helbig, R. Impurity Transition in the Photoluminescence Spectra of SnO_2. *Solid State Commun.* **33**, *1980*, 341–344.
40. Kar, A.; Stroscio, M. A.; Dutta, M.; Kumari, J.; Meyyappan, M. Observation of Ultraviolet Emission and Effect of Surface States on the Luminescence from Tin Oxide Nanowires. *Appl. Phys. Lett.* **2009**, *94*, 101905.
41. Meyer, B. K.; Alves1, H. D.; Hofmann, M.; Kriegseis, W.; Forster, D.; Bertram, F.; Christen, J.; Hoffmann, A.; Straβburg, M.; Dworzak, M.; Haboeck, U.; Rodina, A. V. Bound Exciton and Donor−Acceptor Pair Recombinations in ZnO. *Phys. Status Solidi B* **2004**, *241*, 231–260.
42. Haupt, M.; Ladenburger, A.; Sauer, R.; Thonke, K.; Glass, R.; Roos, W.; Spatz, J. P.; Riethmüller, S.; Möller, M. Ultraviolet-Emitting ZnO Nanowhiskers Prepared by a Vapor Transport Process on Prestructured Surfaces with Self-Assembled Polymers. *J. Appl. Phys.* **2003**, *93*, 6252–6257.
43. Jeong, I. S.; Kim, J. H.; Ima, S. Ultraviolet-Enhanced Photodiode Employing n-ZnO/p-Si Structure. *Appl. Phys. Lett.* **2003**, *83*, 2946–2948.
44. Govender, K.; Boyle, D. S.; O'Brien, P.; Binks, D.; West, D.; Coleman, D. Room- Temperature Lasing Observed from ZnO Nanocolumns Grown by Aqueous Solution Deposition. *Adv. Mater.* **2002**, *14*, 1221–1224.
45. Cao, H.; Xu, J. Y. Y.; Ling, Y.; Burin, A. L.; Seeling, E. W.; Liu, X.; Chang, R. P. H. Random Lasers with Coherent Feedback. *IEEE J. Sel. Top. Quantum Electron* **2003**, *9*, 111–119.
46. Yang, H. Y.; Lau, S. P.; Yu, S. F.; Abiyasa, A. P.; Tanemura, M.; Okita, T.; Hatano, H. High-Temperature Random Lasing in ZnO Nanoneedles. *Appl. Phys. Lett.* **2006**, *89*, 011103.
47. Greene, L. E.; Law, M.; Tan, D. H.; Montano, M.; Goldberger, J.; Somorjai, G.; Yang, P. D. General Route to Vertical ZnO Nanowire Arrays Using Textured ZnO Seeds. *Nano Lett.* **2005**, *5*, 1231–1236.